

Recent τ physics at BaBar

B. Oberhof^a,

on behalf of the BaBar collaboration.

^aUniversità di Pisa & INFN, Pisa, Italy.

Abstract

We report some new results on τ decays obtained by the BaBar collaboration using 468 fb^{-1} of e^+e^- collisions recorded at the PEP-II asymmetric collider at Stanford Linear Accelerator Center. First we will show the results for the branching fractions for the decay of the τ to a charged hadron and two K_S^0 , $\tau^- \rightarrow h^- K_S^0 K_S^0 (\pi^0) \nu_\tau$ and the branching fractions for high-multiplicity decays with 3 or 5 charged particles in the final state, either pions or kaons. We will then show the results for the search of 2^{nd} class hadronic current decays involving η' mesons and the invariant mass spectra for $\tau^- \rightarrow h^- h^+ h^- \nu_\tau$ decays, where $h = \pi, K$.

Keywords: Taus, Tau Decays

1. Introduction

The decays of the τ lepton can be used as a high-precision probe of the Standard Model (SM) and various models of new physics. Last generation B-factories, due to the high luminosity and high $\tau^+\tau^-$ pair production cross section, offer an ideal environment for these studies [1].

As a first result we will present the measurements of the branching fractions of $\tau^- \rightarrow \pi^- K_S^0 K_S^0 (\pi^0) \nu_\tau$ decays and the first search for $\tau^- \rightarrow K^- K_S^0 K_S^0 (\pi^0) \nu_\tau$ decays. The first two of these decays represent a major background for the search of CP violation in the decay rate asymmetry of $\tau^- \rightarrow \pi^- K_S^0 \nu_\tau$ [2], and, due to the large uncertainty on the branching fraction [3], its precise determination is important for future experiments aiming to measure CP violation in τ decays.

Study of the three- and five-prong, where prong means charged track, either pion or kaon, decay modes of the τ lepton, allows one to test the Standard Model and search for evidence of new physics [4]. We present measurements of the (resonant) $\tau^- \rightarrow \pi^- \pi^+ \pi^- \eta \nu_\tau$, $\tau^- \rightarrow \pi^- \pi^+ \pi^- \omega \nu_\tau$, $\tau^- \rightarrow \pi^- f_1 \nu_\tau$ branching fractions. For this purpose we use the primary decay modes of the η , $\omega(782)$, and $f_1(1258)$: $\eta \rightarrow \gamma\gamma$, $\eta \rightarrow \pi^+ \pi^- \pi^0$, $\eta \rightarrow 3\pi^0$; $\omega \rightarrow \pi^+ \pi^- \pi^0$ and $f_1 \rightarrow 2\pi^+ 2\pi^-$, $f_1 \rightarrow \pi^+ \pi^- \eta$. We measure the branching fractions of the non-resonant decays, where the non-resonant category includes possible contributions from broad resonances. We present a new limit on the branching fractions of the second-class current decay $\tau^- \rightarrow \pi^- \eta' (958) \nu_\tau$, and the first limits on the allowed first-class current decays $\tau^- \rightarrow K^- \eta' (958) \nu_\tau$ and $\tau^- \rightarrow \pi^- \pi^0 \eta' (958) \nu_\tau$. We set also the first limits on the branching fractions of five-prong decay modes in which one or more of the charged hadrons is a charged kaon. In all high multiplicity measurements we exclude the contribution of $K_S^0 \rightarrow \pi^+ \pi^-$ decays.

Finally we present the results for the exclusive invariant mass distributions for the decays $\tau^- \rightarrow \pi^- \pi^+ \pi^- \nu_\tau$, $\tau^- \rightarrow K^- \pi^+ \pi^- \nu_\tau$, $\tau^- \rightarrow K^- K^+ \pi^- \nu_\tau$ and $\tau^- \rightarrow K^- K^+ K^- \nu_\tau$. These decays contain a rich and interesting spectrum of low energy QCD resonances and provide a clean environment to probe low energy QCD and measure fundamental properties of the Standard Model [5]. The measurements of the strange spectral function obtained from τ lepton decays to final states containing kaons, for example, can be used for a combined fit of the strange quark mass, m_s , and the Cabibbo Kobayashi Maskawa (CKM) matrix element $|V_{us}|$ [6]. Recent measurements of these branching fractions and spectral functions, interpreted in the framework of the OPE and Finite Energy Sum Rules, suggest a value of $|V_{us}|$ that is approximately three standard deviations lower than Standard Model expectations from CKM unitarity [6]. For this analysis detector effects, in particular the resolution, scale and efficiency have been removed using Bayesian Unfolding [7]. The decay structure for the $\tau^- \rightarrow h^- h^+ h^- \nu_\tau$ is shown both in the unfolded two particle invariant mass distributions and three dimensional distribution which is presented as Dalitz plots in slices of the three body invariant mass along with the projections. These distributions are of particular interest to model builders to study the rich decay structure of the τ lepton.

All these analyses are based on data recorded with the BaBar detector at the PEP-II asymmetric-energy e^+e^- storage rings operated at the SLAC National Accelerator Laboratory. With an integrated luminosity $\mathcal{L} = 424 + 44 \text{ fb}^{-1}$ recorded at center-of-mass (CM) energies of 10.58 GeV and 10.54 GeV, respectively, and an averaged $\tau^+\tau^-$ production cross section of $\sigma_{\tau\tau} = (0.919 \pm 0.003) \text{ nb}$ [1], the data sample amounts to 430 million τ pairs. The BaBar detector is described in detail in Ref. [8]. Charged-particle momenta are measured with a five-layer double-sided silicon vertex tracker and a 40-layer drift chamber, both operating in the 1.5 T magnetic field of a superconducting solenoid. Information from a detector of internally reflected Cerenkov light is used in conjunction with

Email address: benjamin.oberhof@infn.it (on behalf of the BaBar collaboration.)

specific energy loss measurements from the tracking detectors to identify charged pions and kaons [9]. Photons are reconstructed from energy clusters deposited in a CsI(Tl) electromagnetic calorimeter. Electrons are identified by combining tracking and calorimeter information. An instrumented magnetic flux return is used to identify muons. The background contamination and selection efficiencies are determined using Monte Carlo simulation. The τ -pair production is simulated with the KK2F event generator [10]. The τ decays, continuum $q\bar{q}$, events, and final-state radiative effects are modeled with the Tauola [11], JETSET [12], and Photos [13] generators, respectively. The detector response is simulated with GEANT4 [14]. All Monte Carlo events are processed through a full simulation of the BaBar detector and are reconstructed in the same manner as data.

2. The branching fraction of $\tau^- \rightarrow h^- K_S^0 K_S^0 (\pi^0) \nu_\tau$ decays

The $\tau^- \rightarrow \pi^- K_S^0 K_S^0 \nu_\tau$ decay is simulated with Tauola using $\tau^- \rightarrow K^{*-} K^0 \nu_\tau$. The $\tau^- \rightarrow \pi^- K_S^0 K_S^0 \pi^0 \nu_\tau$ decay is simulated with EVTGEN using $\tau^- \rightarrow K^{*-} K^0 \pi^0 \nu_\tau$ and $\tau^- \rightarrow \pi^- K^{*0} K^0 \nu_\tau$. As we will see the $\tau^- \rightarrow K^{*-} K^0 \nu_\tau$ and $\tau^- \rightarrow K^{*0} K^0 \nu_\tau$ have a $K^*(892)$ meson that is observed in the $\pi^- K_S^0$ channel, while the $\tau^- \rightarrow \pi^- K^{*0} K^0 \nu_\tau$ has a $K^{*0}(892)$ meson that is observed in $\pi^0 K_S^0$ channel. The decay products of the two τ leptons can be separated from each other by dividing the event into two hemispheres using the plane perpendicular to the event thrust axis [12]. The thrust axis is calculated using all charged particles and all neutral deposits event. We select events with one prompt track, with closest approach to the beam spot less than 1.5 cm in the plane transverse to the beam axis and 2.5 cm in the longitudinal direction, and two reconstructed K_S^0 candidates in the signal hemisphere. In the other hemisphere we require one oppositely charged track.

A K_S^0 candidate is defined as a pair of oppositely charged tracks, with an invariant mass between 0.475 and 0.525 GeV/c^2 (fig. 2).

The charged pion and kaon samples are divided into samples with zero and one π^0 mesons. Events with two or more π^0 mesons are rejected. π^0 candidate are reconstructed from two clusters in the calorimeter, with a minimum energy of 30 MeV, and an invariant mass between 0.115 GeV/c^2 and 0.150 GeV/c^2 . To reduce backgrounds from non- τ -pair events, we require the momentum of the charged particle in the tag hemisphere to be less than 4 GeV/c in the CM frame and to be identified either as an electron or a muon.

The invariant mass of the charged hadron and the two K_S^0 mesons is required to be less than 1.8 GeV/c^2 . The $\pi^- K_S^0 K_S^0$ invariant mass distributions are shown in fig. 2. The invariant mass distribution predicted by the MC for the hadronic final state particles and for their combinations do not perfectly describe the data. In particular, the peak of the invariant mass distribution in the MC is found to peak approximately 5% lower than the peak observed in the data. To improve the modeling of the data we have weighted the $\tau^- \rightarrow \pi^- K_S^0 K_S^0 \nu_\tau$ in Tauola using the Dalitz plot distribution for the $K_S^0 \pi^-$ invariant mass

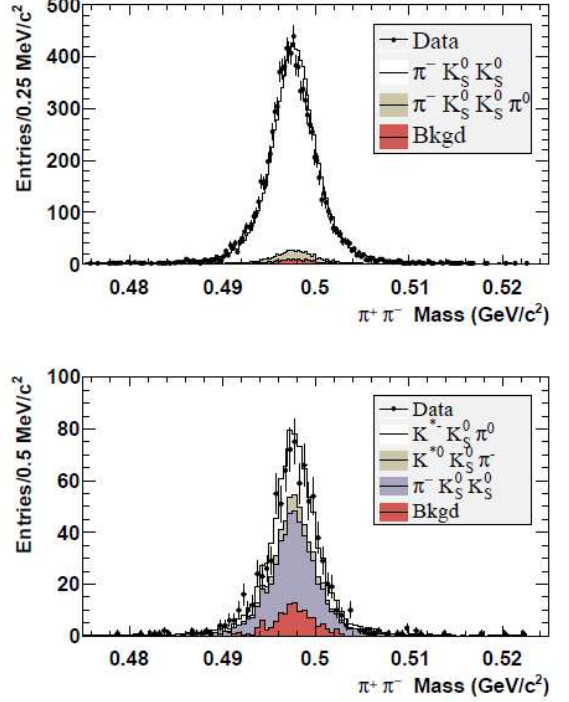


Figure 1: The invariant mass of the two $K_S^0 \rightarrow \pi^+ \pi^-$ candidates for the $\tau \rightarrow \pi K_S^0 K_S^0 \nu_\tau$ (top) and $\tau \rightarrow \pi K_S^0 K_S^0 \pi^0 \nu_\tau$ (bottom) samples after selection. The points are data and the histograms are the prediction of the Monte Carlo simulation. For both plots, the white histogram represents $\tau^- \rightarrow K^{*-} K^0 \nu_\tau$ decays, the blue and beige histogram shows the $\tau^- \rightarrow K^{*0} K^0 \pi^0 \nu_\tau$ and $\tau^- \rightarrow K^{*0} K^0 \pi^- \nu_\tau$ decays, respectively while the red histogram is the $q\bar{q}$ background.

of fig. 2. The weighted events are used in all the mass plots and we observe an improvement in the modeling of the data. The branching fractions of the two charged pion modes are determined simultaneously to take into account the cross feed of each decay mode into the other sample.

Table 1 summarizes the number of data and background events for each reconstruction mode as well as the selection efficiency matrix.

We measure the $\tau^- \rightarrow \pi^- K_S^0 K_S^0 \nu_\tau$ and $\tau^- \rightarrow \pi^- K_S^0 K_S^0 \pi^0 \nu_\tau$ branching fractions to be:

$$B(\tau^- \rightarrow \pi^- K_S^0 K_S^0 \nu_\tau) = (2.31 \pm 0.04 \pm 0.08) \times 10^{-4} \quad (1)$$

and

$$B(\tau^- \rightarrow \pi^- K_S^0 K_S^0 \pi^0 \nu_\tau) = (1.60 \pm 0.20 \pm 0.22) \times 10^{-5} \quad (2)$$

respectively.

The systematic uncertainties are divided into the selection efficiency, background, and common systematic components. The selection efficiencies include the MC statistical error and an error that takes into account the uncertainty for finding a fake π^0 meson. The background is predicted by the MC simulation to be entirely from $e^+ e^- \rightarrow q\bar{q}$ events and is confirmed with data and MC simulation control samples. The control samples are created using the nominal selection criteria except that the invariant mass requirements are reversed to eliminate the τ pair events and enhance $q\bar{q}$ events. The ratio of selected events in

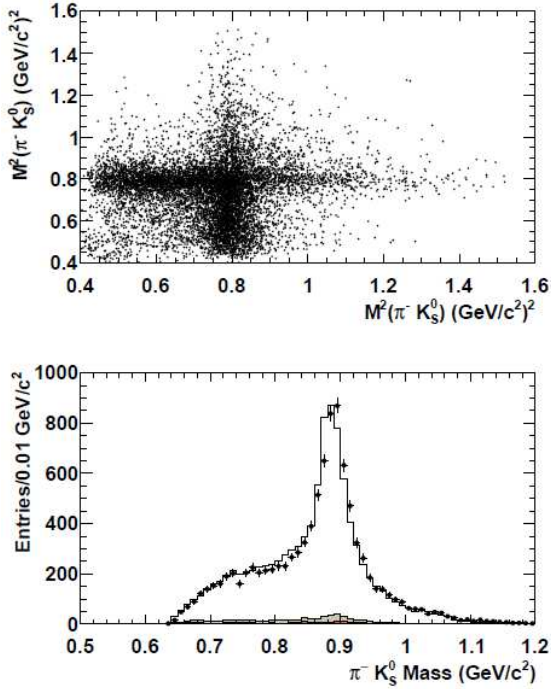


Figure 2: The Dalitz plot and the invariant mass distributions for of the $K_S^0\pi^-$ system of selected events. There are two entries per event in the Dalitz plot and in the $K_S^0\pi^-$ mass plot. The points are data and the histograms are the prediction of the Monte Carlo simulation. The white histogram represents $\tau^- \rightarrow K^{*0}K^0\nu_\tau$ decays, the blue and beige histogram shows the $\tau^- \rightarrow K^{*0}K^0\pi^0\nu_\tau$ and $\tau^- \rightarrow K^{*0}K^0\pi^-\nu_\tau$ decays, respectively while the red histogram is the $q\bar{q}$ background.

the data to MC control samples is found to be consistent with unity within 15% for both samples. The 15% value is added to the MC statistical uncertainty of the number of background events. A number of systematic uncertainties are common to both branching fractions measurements. They can be categorized into two components: tracking and particle identification reconstruction uncertainties, and topological selection uncertainties. The tracking and particle identification reconstruction uncertainties include the uncertainty on the track reconstruction efficiency (0.5%) and the uncertainties on the efficiencies for particle identification: lepton identification (combined electron and muon) (1.6%), charged pion particle identification (0.5%), and K_S^0 identification (1.8%). The topological selection uncertainties include a 2% uncertainty associated with the selection criteria. The uncertainty on the number of τ pairs given by the product of the luminosity and the $e^+e^- \rightarrow \tau^+\tau^-$ cross section is also included (1%).

The same criteria are used to select $\tau^- \rightarrow \pi^-K_S^0K_S^0\nu_\tau$ and $\tau^- \rightarrow \pi^-K_S^0K_S^0\pi^0\nu_\tau$ decays except that the charged track is required to be a kaon. The numbers of events are given in table 2 and are found to be consistent with the estimated background prediction. The background is almost entirely due to cross feed of decays and very little contribution from $q\bar{q}$ events. The branching fractions are determined for each channel independently and used to place upper limits on the branching fractions of:

$$B(\tau^- \rightarrow \pi^-K_S^0K_S^0\nu_\tau) < 6.3 \times 10^{-7} \quad (3)$$

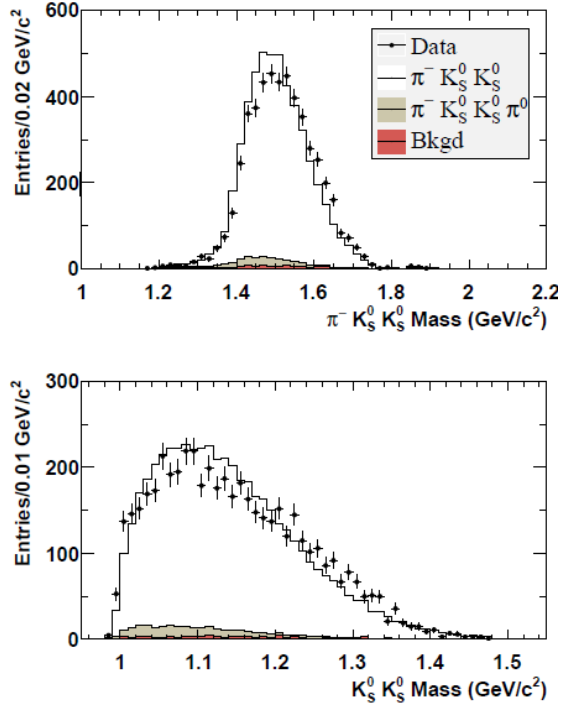


Figure 3: Invariant mass distributions for events that pass the selection criteria. The invariant mass requirement is not required for the plot of the $K_S^0K_S^0\pi^-$ invariant mass. The points are data and the histograms are the prediction of the Monte Carlo simulation. The white histogram represents $\tau^- \rightarrow K^{*0}K^0\nu_\tau$ decays, the blue and beige histogram shows the $\tau^- \rightarrow K^{*0}K^0\pi^0\nu_\tau$ and $\tau^- \rightarrow K^{*0}K^0\pi^-\nu_\tau$ decays, respectively while the red histogram is the $q\bar{q}$ background. The mass plots use $\tau^- \rightarrow K_S^0K_S^0\nu_\tau$ events that have been weighted based on the Dalitz plot distributions.

and

$$B(\tau^- \rightarrow \pi^-K_S^0K_S^0\pi^0\nu_\tau) < 4.0 \times 10^{-7} \quad (4)$$

at the 90% confidence level.

3. High multiplicity τ decays

We select events where one hemisphere (tag) contains exactly one track while the other hemisphere (signal) contains exactly three or five tracks with total charge opposite to that of the tag hemisphere. The event is rejected if any pair of oppositely charged tracks is consistent with a photon conversion. All tracks are required to have a point of closest approach to the interaction region less than 1.5 cm in the plane transverse to the beam axis and less than 2.5 cm in the direction along that axis in order to reject tracks coming from K_S^0 decays. To reduce backgrounds from non- τ -pair events, we require that the momentum of the charged particle in the tag hemisphere be less than 4GeV/c in the CM frame and that the charged particle be identified as an electron or a muon. The $q\bar{q}$ background is suppressed by requiring that there be at most one energetic ($E > 1\text{GeV}$) electromagnetic calorimeter cluster in the tag hemisphere that is not associated with a track. Additional background suppression is achieved by requiring the magnitude of the event thrust to lie between 0.92 and 0.99. Neutral pion candidates

	$\tau^- \rightarrow \pi^- K_S^0 K_S^0 \nu_\tau$	$\tau^- \rightarrow \pi^- K_S^0 K_S^0 \pi^0 \nu_\tau$
Branching Fraction (10^{-5})	$(23.1 \pm 0.4 \pm 0.8)$	$(1.60 \pm 0.20 \pm 0.22)$
Data Events	4985	409
Estimated Background	98 ± 17	35 ± 7
Efficiency:		
$\tau^- \rightarrow \pi^- K_S^0 K_S^0 \nu_\tau$	$(4.93 \pm 0.02) \%$	$(0.21 \pm 0.01) \%$
$\tau^- \rightarrow \pi^- K_S^0 K_S^0 \pi^0 \nu_\tau$	$(3.04 \pm 0.10) \%$	$(2.65 \pm 0.09) \%$
Selection Efficiency	0.008	0.12
Background	0.004	0.04
Common Contributions	0.034	0.03
Total	0.035	0.13

Table 1: Results for the charged pion decays including relative systematic contribution to the total error.

	$\tau^- \rightarrow K^- K_S^0 K_S^0 \nu_\tau$	$\tau^- \rightarrow K^- K_S^0 K_S^0 \pi^0 \nu_\tau$
Branching Fraction (10^{-7})	$(1.90 \pm 3.00 \pm 0.03)$	$(1.50 \pm 1.80 \pm 0.10)$
Limit at 90% CL	6.3×10^{-7}	4.0×10^{-7}
Data Events	23	1
Estimated Background	20 ± 0.50	0.15 ± 0.02
Efficiency:	$(3.85 \pm 0.04) \%$	$(1.37 \pm 0.03) \%$

Table 2: Results for the charged kaon decays.

are reconstructed in the signal hemisphere. If a photon candidate meets the invariant mass requirement with multiple photon candidates, then the neutral pion candidate with invariant mass closest to the nominal π^0 mass is selected. The search for additional pion candidates is then repeated using the remaining photon candidates. The residual photon clusters in the signal hemisphere are used to search for $\eta \rightarrow \gamma\gamma$ candidates. The branching fractions are calculated using the expression $B = N_S / (2N_{\tau\tau}\epsilon)$ where N_S is the number of candidates after background subtraction, $N_{\tau\tau}$ is the number of τ pairs produced, and ϵ is the selection efficiency. The uncertainty of N is estimated to be 1%. The selection efficiencies are determined from the signal Monte Carlo samples. The uncertainty on the selection efficiencies includes 0.5% per track on the track reconstruction efficiency, as well as particle identification (PID) selection uncertainties. From studies conducted on real and simulated events, the uncertainties on the charged particle identification selectors are estimated to be 1% for electrons, 2.5% for muons, 0.5% for pions, and 1.8% for kaons. The combined electron and muon particle identification uncertainty is estimated to be 1.6% based on the composition of the event samples. The uncertainty on the $\pi^0 \rightarrow \gamma\gamma$ and $\eta \rightarrow \gamma\gamma$ reconstruction efficiency is estimated to be 3% per candidate.

3.1. Resonant high multiplicity τ decays

3.1.1. $\tau^- \rightarrow 3(\pi^-)\eta\nu_\tau$

The $\tau^- \rightarrow \pi^- \pi^+ \pi^- \eta \nu_\tau$ mode is studied in the $\eta \rightarrow \gamma\gamma$, $\eta \rightarrow \pi^- \pi^+ \pi^0$, and $\eta \rightarrow 3\pi^0$ final states, while the $\tau^- \rightarrow \pi^- 2\pi^0 \eta \nu_\tau$ mode is studied in the $\eta \rightarrow \pi^- \pi^+ \pi^0$ final state. The event yields are determined by fitting the η mass peak in the invariant mass distributions (fig. 3.1.1). The Monte Carlo simulation indi-

cates that some of the entries in the peak are from $e^+e^- \rightarrow q\bar{q}$ events. Control samples, obtained by reversing the require-

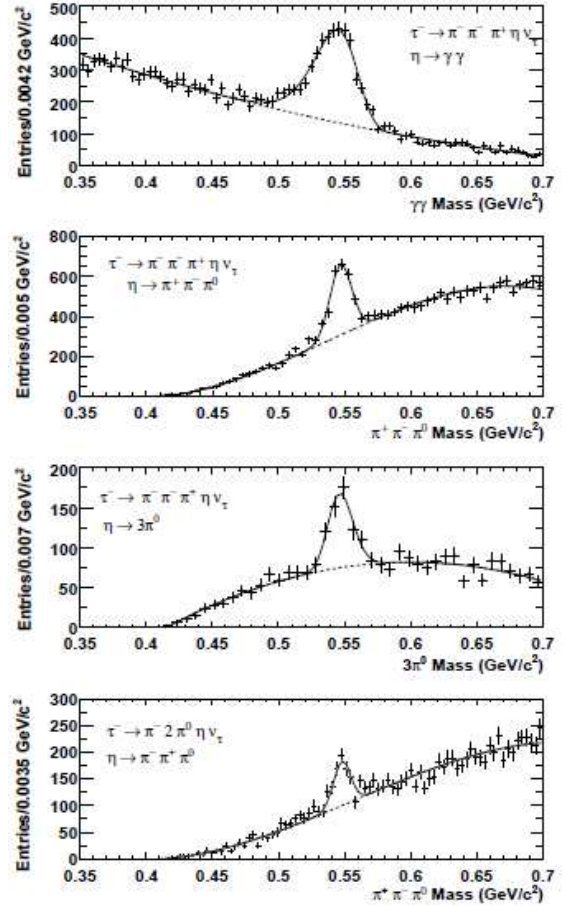


Figure 4: The $\gamma\gamma$, $\pi^+\pi^-\pi^0$, and $3\pi^0$ invariant mass distributions for $\tau^- \rightarrow \pi^- \pi^+ \pi^- \eta \nu_\tau$ candidates, and the $\pi^+\pi^-\pi^0$ invariant mass distribution for $\tau^- \rightarrow \pi^- 2\pi^0 \eta \nu_\tau$ decay candidates, after all selection criteria are applied. The solid lines represent the fit to the η peak and background. The dashed lines show the extrapolation of the background function under the η peak.

ment on the invariant mass, are used to validate the background estimate. The expected background is corrected by the ratio of data to Monte Carlo events, and the statistical uncertainty of the ratio is included in the background systematic uncertainty. This method of validating the $q\bar{q}$ background estimate is used for all decays and is not mentioned in the later sections. The reconstruction efficiencies are determined from fits to the signal Monte Carlo samples. The three determinations of the $\tau^- \rightarrow \pi^- \pi^+ \pi^- \eta \nu_\tau$ branching fraction are found to be in good agreement and we therefore calculate a weighted average. The weighted average is found to be

$$B(\tau^- \rightarrow \pi^- \pi^+ \pi^- \eta \nu_\tau) = (2.25 \pm 0.07 \pm 0.12) \times 10^{-4}. \quad (5)$$

The $\tau^- \rightarrow \pi^- 2\pi^0 \eta \nu_\tau$ branching fraction, in turn, is found to be

$$B(\tau^- \rightarrow \pi^- 2\pi^0 \eta \nu_\tau) = (2.01 \pm 0.34 \pm 0.22) \times 10^{-4}. \quad (6)$$

Naively, the ratio of the $\tau^- \rightarrow \pi^- \pi^+ \pi^- \eta \nu_\tau$ to $\tau^- \rightarrow \pi^- 2\pi^0 \eta \nu_\tau$ branching fractions is expected to be two if the decay is dominated by the $\tau^- \rightarrow \pi^- f_1 \nu_\tau$ decay mode. The data do not support

this expectation. The measurements are in good agreement with the results from the CLEO Collaboration, $(2.3 \pm 0.5) \times 10^{-4}$ and $(1.5 \pm 0.5) \times 10^{-4}$, for $\tau^- \rightarrow \pi^- \pi^+ \pi^- \eta \nu_\tau$ and $\tau^- \rightarrow \pi^- 2\pi^0 \eta \nu_\tau$ respectively [15].

Table 3 summarizes the results for the individual channels.

	BF in 10^{-4}	N_S	N_{bkg}	ϵ (%)
$\tau^- \rightarrow \pi^- \pi^+ \pi^- \eta \nu_\tau$				
$\eta \rightarrow \gamma\gamma$	$2.10 \pm 0.09 \pm 0.13$	2887 ± 103	131 ± 29	3.83 ± 0.11
$\tau^- \rightarrow \pi^- \pi^+ \pi^- \eta \nu_\tau$				
$\eta \rightarrow \pi^+ \pi^- \pi^0$	$2.37 \pm 0.12 \pm 0.18$	1440 ± 68	65 ± 38	2.97 ± 0.12
$\tau^- \rightarrow \pi^- \pi^+ \pi^- \eta \nu_\tau$				
$\eta \rightarrow 3\pi^0$	$2.54 \pm 0.27 \pm 0.25$	315 ± 34	13 ± 7	0.42 ± 0.01
$\tau^- \rightarrow \pi^- \pi^+ \pi^- \eta \nu_\tau$	$2.01 \pm 0.34 \pm 0.22$	381 ± 45	83 ± 12	05.7 ± 0.02

Table 3: Results and branching fractions for $\tau^- \rightarrow (3\pi)^- \eta \nu_\tau$ decays.

3.1.2. $\tau^- \rightarrow \pi^- f_1 \nu_\tau$

The branching fraction of $\tau^- \rightarrow \pi^- f_1 \nu_\tau$ as well as the f_1 mass are measured using the $f_1 \rightarrow 2\pi^+ 2\pi^-$ and $f_1 \rightarrow \pi^+ \pi^- \eta$ decay modes, where the last one is reconstructed using $\eta \rightarrow \gamma\gamma$, $\eta \rightarrow \pi^+ \pi^- \pi^0$, and $\eta \rightarrow 3\pi^0$ events. With respect to the selection criteria already described we modify the selection for the mass measurement, dropping the requirement that the track in the tag hemisphere be a lepton and the restriction on the number of photon candidates in the tag hemisphere, in order to increase the size of the event sample. The numbers of $\tau^- \rightarrow \pi^- f_1 \nu_\tau$ candidates are determined by fitting the f_1 peak in the $2\pi^+ 2\pi^-$ and $\pi^+ \pi^- \pi^0$ invariant mass distributions. The f_1 lineshape is expected to be a Breit-Wigner distribution, modified by the limited phase space. Previous studies show that the $f_1 \rightarrow a_0^- \pi^+$, ($a_0^- \rightarrow \pi^- \eta$ channel accounts for all $f_1 \rightarrow \pi^+ \pi^- \eta$ decays [16]. The mass of the $\pi^+ a_0^-(980)$ system and the τ mass provide a lower and upper limit, respectively, on the f_1 lineshape. We use EVTGEN generator to determine the simulated f_1 lineshape and find it to be a close approximation to the Breit-Wigner expectation. The f_1 peak is fit using this lineshape convolved with a Gaussian distribution to take into account the effects of the detector resolution.

The product of the $\tau^- \rightarrow \pi^- f_1 \nu_\tau$ and $f_1 \rightarrow 2\pi^+ 2\pi^-$ branching fractions, and the product of the $\tau^- \rightarrow \pi^- f_1 \nu_\tau$ and $f_1 \rightarrow \pi^+ \pi^- \eta$ branching fractions, are measured to be

$$B(\tau^- \rightarrow \pi^- f_1 \nu_\tau) B(f_1 \rightarrow 2\pi^+ 2\pi^-) = \quad (7)$$

$$(5.20 \pm 0.31 \pm 0.37) \times 10^{-5} \quad (8)$$

$$B(\tau^- \rightarrow \pi^- f_1 \nu_\tau) B(f_1 \rightarrow \pi^+ \pi^- \eta) = \quad (9)$$

$$(1.26 \pm 0.06 \pm 0.06) \times 10^{-4} \quad (10)$$

respectively, where the second result is the weighted average of the three η modes. The $B(\tau^- \rightarrow \pi^- f_1 \nu_\tau)$ branching fraction is determined to be $(4.73 \pm 0.28 \pm 0.45) \times 10^{-4}$ and $(3.60 \pm 0.18 \pm 0.23) \times 10^{-4}$, as obtained by dividing the product branching fractions by $B(f_1 \rightarrow 2\pi^+ 2\pi^-) = 0.110^{+0.007}_{-0.006}$ and $B(f_1 \rightarrow \pi^+ \pi^- \eta) = 0.349^{+0.013}_{-0.015}$ [17], respectively.

Table 4 summarizes the results for the individual channels.

	BF in 10^{-4}	N_S	ϵ (%)
$f_1 \rightarrow 2\pi^+ 2\pi^-$	$0.520 \pm 0.031 \pm 0.037$	3722 ± 222	8.3 ± 0.1
$f_1 \rightarrow \pi^+ \pi^- \eta$			
$\eta \rightarrow \gamma\gamma$	$1.25 \pm 0.08 \pm 0.07$	1605 ± 94	2.97 ± 0.12
$f_1 \rightarrow \pi^+ \pi^- \eta$			
$\eta \rightarrow \pi^+ \pi^- \pi^0$	$1.26 \pm 0.11 \pm 0.08$	731 ± 62	2.97 ± 0.05
$f_1 \rightarrow \pi^+ \pi^- \eta$			
$\eta \rightarrow 3\pi^0$	$1.33 \pm 0.34 \pm 0.39$	197 ± 59	0.53 ± 0.06

Table 4: Results and branching fractions for $\tau^- \rightarrow \pi^- f_1 \nu_\tau$ decays.

The f_1 mass is determined by fitting the peak with a non-relativistic Breit-Wigner function, which was used in previous measurements of the f_1 mass [17]. As a cross check, we use the energy-momentum four-vectors from the generator Monte Carlo simulation, and we find the fitted mass value to be consistent with the input mass value. The results for the different channels are shown in fig. 3.1.2.

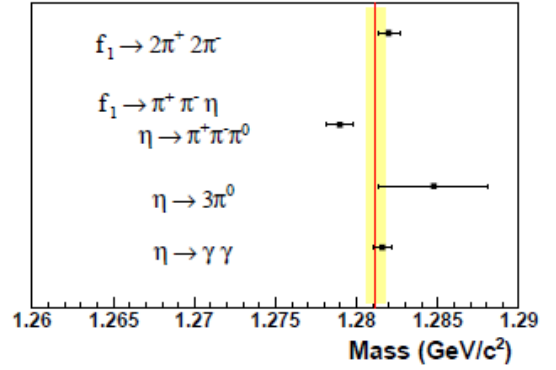


Figure 5: Compilation of our measurements of the f_1 mass. The solid line is the weighted average and the shaded area is the one-standard-deviation region.

We determine the mass of the $f_1(1258)$ meson to be

$$M_{f_1} = (1.28116 \pm 0.00039 \pm 0.00045) \text{ GeV}/c^2. \quad (11)$$

The systematic uncertainty includes the reconstruction uncertainty and the calibration uncertainty. This result is in good agreement with the value $(1.2818 \pm 0.0006) \text{ GeV}/c^2$ in [17].

3.1.3. $\tau^- \rightarrow 3(\pi)^- \omega \nu_\tau$

We measure the $\tau^- \rightarrow \pi^+ 2\pi^- \omega \nu_\tau$ and $\tau^- \rightarrow \pi^- 2\pi^0 \omega \nu_\tau$ branching fractions. The number of events is determined by fitting the η peak in the $\pi^+ \pi^- \pi^0$ invariant mass distributions with a Breit-Wigner distribution, which is convolved with a Gaussian distribution to take into account the detector resolution. A polynomial function is used to fit the background. The results are presented in 5. Approximately 10% of the events in the $\tau^- \rightarrow \pi^+ 2\pi^- \omega \nu_\tau$ channel are backgrounds from other τ decays (primarily $\tau^- \rightarrow \pi^- \pi^0 \omega \nu_\tau$ decays) and $e^+ e^- \rightarrow q\bar{q}$ events. The backgrounds are subtracted before calculating the branching fraction. The $\tau^- \rightarrow \pi^- 2\pi^0 \omega \nu_\tau$ sample has substantial contributions from $\tau^- \rightarrow \pi^- \omega \nu_\tau$ and $\tau^- \rightarrow \pi^- \pi^0 \omega \nu_\tau$ decays. The

background is estimated with the Monte Carlo simulation and verified using data and simulation control samples. The control samples follow the nominal selection criteria but select one or two π^0 instead of three π^0 mesons. The branching fractions are found to be

$$B(\tau^- \rightarrow \pi^+ 2\pi^- \omega \nu_\tau) = (8.4 \pm 0.4 \pm 0.6) \times 10^{-5} \quad (12)$$

$$B(\tau^- \rightarrow \pi^- 2\pi^0 \omega \nu_\tau) = (7.3 \pm 1.2 \pm 1.2) \times 10^{-5}. \quad (13)$$

	$\tau^- \rightarrow \pi^+ 2\pi^- \omega \nu_\tau$	$\tau^- \rightarrow \pi^- 2\pi^0 \omega \nu_\tau$
Branching Fraction	$(8.4 \pm 0.4 \pm 0.6) \times 10^{-5}$	$(7.3 \pm 1.2 \pm 1.2) \times 10^{-5}$
Data Events	2372 ± 94	1135 ± 70
Estimated Background	257 ± 71	709 ± 59
Efficiency:	$(3.27 \pm 0.03) \%$	$(0.75 \pm 0.01) \%$

Table 5: Results and branching fractions for $\tau^- \rightarrow 3(\pi^-) \omega \nu_\tau$ decays.

3.2. Nonresonant high multiplicity τ decays

The resonant modes, involving η , ω and f_1 mesons, do not account for all of the observed decays. We consider the excess in the observed decays to be from non-resonant modes. We make no attempt to identify the contribution of resonances with widths larger than 100 MeV/c² as the nature of these resonances is complex and their lineshapes will be modified by the limited phase space. We measure the branching fractions of the non resonant $\tau^- \rightarrow \pi^+ 2\pi^- 3\pi^0 \nu_\tau$, $\tau^- \rightarrow 2\pi^+ 3\pi^- \nu_\tau$ and $\tau^- \rightarrow 2\pi^+ 3\pi^- \pi^0 \nu_\tau$ decays. The numbers of candidates are given by the numbers of events found in the data after subtracting the resonant contributions and the background from other τ decays and $q\bar{q}$ events. The resonant decays dominate the $\tau^- \rightarrow \pi^+ 2\pi^- 3\pi^0 \nu_\tau$ mode. The background is primarily from $\tau^- \rightarrow \pi^- \pi^0 \omega \nu_\tau$ and $q\bar{q}$ events. The branching fraction of this non-resonant mode is determined to be

$$B(\tau^- \rightarrow \pi^+ 2\pi^- 3\pi^0 \nu_\tau) = (1.0 \pm 0.8 \pm 3.0) \times 10^{-5}. \quad (14)$$

The systematic uncertainty on the branching fraction is dominated by the uncertainty in the background, which includes the Monte Carlo statistical uncertainty and the τ branching fraction uncertainties. The branching fraction is consistent with zero and we set a limit of

$$B(\tau^- \rightarrow \pi^+ 2\pi^- 3\pi^0 \nu_\tau) < 5.8 \times 10^{-5}. \quad (15)$$

at 90% confidence level. We also determine the inclusive $\tau^- \rightarrow \pi^+ 2\pi^- 3\pi^0 \nu_\tau$ branching fraction, given by the sum of the resonant and non-resonant terms. We find the result

$$B(\tau^- \rightarrow \pi^+ 2\pi^- 3\pi^0 \nu_\tau) = (2.07 \pm 0.18 \pm 0.37) \times 10^{-4} \quad (16)$$

where the systematic uncertainty accounts for correlations between the systematic uncertainties of the individual modes.

The $\tau^- \rightarrow 2\pi^+ 3\pi^- \nu_\tau$ decay has only a small contribution from resonant decays. The branching fraction is determined to be

$$B(\tau^- \rightarrow 2\pi^+ 3\pi^- \nu_\tau) = (7.68 \pm 0.04 \pm 0.40) \times 10^{-4}. \quad (17)$$

Although the modeling of the $2\pi^+ 3\pi^-$ invariant mass distribution is deficient, the selection efficiency remains the same if the Monte Carlo is re-weighted to resemble the data distribution. The inclusive branching fraction is

$$B(\tau^- \rightarrow 2\pi^+ 3\pi^- \nu_\tau) = (8.33 \pm 0.04 \pm 0.43) \times 10^{-4} \quad (18)$$

and is obtained by adding the non-resonant branching fraction with the resonant branching fraction for the $\tau^- \rightarrow \pi^- f_1 \nu_\tau$ via $f_1 \rightarrow 2\pi^+ 2\pi^-$ decay.

$\tau^- \rightarrow 2\pi^+ 3\pi^- \pi^0 \nu_\tau$ decays are dominated by the resonant modes. We determine the branching fraction of the non-resonant $\tau^- \rightarrow 2\pi^+ 3\pi^- \pi^0 \nu_\tau$ decay to be

$$B(\tau^- \rightarrow 2\pi^+ 3\pi^- \pi^0 \nu_\tau) = (3.6 \pm 0.3 \pm 0.9) \times 10^{-5}. \quad (19)$$

The systematic uncertainty on this non-resonant branching fraction is dominated by the large uncertainty in the background. Although the invariant mass distributions of the resonant modes in the Monte Carlo simulation are corrected to provide better agreement with the data, the corrections make little difference to the final branching fraction result. The other τ decays and the $q\bar{q}$ events contribute to a lesser extent; their contribution to the uncertainty of the background is very small. The inclusive branching fraction

$$B(\tau^- \rightarrow 2\pi^+ 3\pi^- \pi^0 \nu_\tau) = (1.65 \pm 0.05 \pm 0.09) \times 10^{-4} \quad (20)$$

and is obtained by adding the non-resonant branching fraction and the resonant branching fractions attributed to the $\tau^- \rightarrow 2\pi^- \pi^+ \eta \nu_\tau$ via $\eta \rightarrow \pi^+ \pi^- \pi^0$ and $\tau^- \rightarrow 2\pi^- \pi^+ \omega \nu_\tau$ via $\omega \rightarrow \pi^+ \pi^- \pi^0$ decays.

3.3. 5-prong τ decays with kaons

We present here also the first search for high-multiplicity τ decays with one or two charged kaons. We find no evidence for signal decays and place upper limits on the branching fractions of 5 different decay modes. The events are divided into topologies in which the charged kaon has either the same or opposite charge as the parent τ lepton. If there are two kaon candidates, they must have opposite charge. All other tracks are required to be identified as charged pions. Figure 9 shows the mass spectra for the various channels. The predictions of the Monte Carlo simulation are divided into decays with or without a K. The background estimates, which give the dominant systematic uncertainty, are verified by comparing the numbers of events in the data and Monte Carlo samples in the $M > 1.8$ GeV/c² region. The backgrounds predicted by the Monte Carlo simulation are approximately equal to the numbers of events in the data sample. The upper limits on the branching fractions are given in 6.

Currently there are no theoretical predictions for these modes. We estimate that $B(\tau^- \rightarrow K^- 2\pi^- 2\pi^+ \nu_\tau) \sim 10^{-5} - 10^{-6}$ if the decay is related to $B(\tau^- \rightarrow 3\pi^- 2\pi^+ \nu_\tau)$ by the ratio of the CKM matrix elements (V_{us}/V_{ud}).

	Limit 10^{-6}	N_S	N_{bkg}	ϵ (%)
$\tau^- \rightarrow K^- 2\pi^- 2\pi^+ \nu_\tau$	2.4	1328 ± 36	1284 ± 72	7.9 ± 0.1
$\tau^- \rightarrow K^+ 3\pi^- \pi^+ \nu_\tau$	5	1999 ± 45	1890 ± 163	7.9 ± 0.1
$\tau^- \rightarrow K^- K^+ 2\pi^- \pi^+ \nu_\tau$	0.45	32 ± 6	15 ± 4	6.7 ± 0.1
$\tau^- \rightarrow K^- 2\pi^- 2\pi^+ \pi^0 \nu_\tau$	1.9	112 ± 11	84 ± 10	2.9 ± 0.06
$\tau^- \rightarrow K^+ 3\pi^- \pi^+ \pi^0 \nu_\tau$	0.8	154 ± 12	170 ± 16	2.9 ± 0.06

Table 6: Upper limits at 90% CL for charged kaon decay modes.

4. Search for 2nd class current decays

We show here the results search for the $\tau^- \rightarrow \pi^- \pi^0 \eta'(958) \nu_\tau$, $\tau^- \rightarrow K^- \eta'(958) \nu_\tau$, and $\tau^- \rightarrow \pi^- \eta'(958) \nu_\tau$ decays, where $\eta' \rightarrow \pi^+ \pi^- \eta$. The first two decays are allowed first-class current decays whereas the last decay is a second-class current decay, which rate would be zero in the limit of perfect isospin symmetry. The event selection is similar to the previous sections. For the $\tau^- \rightarrow \pi^- \pi^0 \eta'(958) \nu_\tau$ via $\eta \rightarrow \gamma\gamma$ and the $\tau^- \rightarrow \pi^- \eta'(958) \nu_\tau$ via $\eta \rightarrow \gamma\gamma$ and $\eta \rightarrow \pi^+ \pi^- \pi^0$ modes, we measure the number of η' candidates by fitting the peak with a Gaussian function and the combinatoric background with a polynomial function. The number of η' candidates in the other channels is determined by counting the number of events in a single bin centered on the η' mass and subtracting the combinatorial events. The level of the combinatorial background is estimated by fitting the mass spectrum or from the average level of the sideband region around the η' peak.

We find no evidence for any of these decays and place the following upper limits on the branching fractions at the 90% confidence level:

$$B(\tau^- \rightarrow \pi^- \pi^0 \eta'(958) \nu_\tau) < 1.2 \times 10^{-5} \quad (21)$$

$$B(\tau^- \rightarrow K^- \eta'(958) \nu_\tau) < 2.4 \times 10^{-6} \quad (22)$$

$$B(\tau^- \rightarrow \pi^- \eta'(958) \nu_\tau) < 4.0 \times 10^{-6}. \quad (23)$$

The limits are determined from the weighted average of the branching fractions measured for each mode. The $\tau^- \rightarrow \pi^- \pi^0 \eta'(958) \nu_\tau$ and $\tau^- \rightarrow K^- \eta'(958) \nu_\tau$ channels are potential backgrounds to the $\tau^- \rightarrow \pi^- \eta'(958) \nu_\tau$ decay. We find that background from these two decays is less than two events based on the upper limits on the branching fractions and we consider these backgrounds to be negligible. It is predicted that the branching fraction of $\tau^- \rightarrow \pi^- \eta'(958) \nu_\tau$ should be less than 1.4×10^{-6} [18].

5. $\tau^- \rightarrow h^- h^+ h^- \nu_\tau$ invariant mass spectra

For the event selection, a sample of $\tau^- \rightarrow h^- h^+ h^- \nu_\tau$ decays events is selected by requiring the partner τ^+ to decay leptonically. Within this sample, each of the mesons is uniquely identified as a charged pion or kaon, and the decay categorized as $\tau^- \rightarrow \pi^- \pi^+ \pi^- \nu_\tau$, $\tau^- \rightarrow K^- \pi^+ \pi^- \nu_\tau$, $\tau^- \rightarrow K^- K^+ \pi^- \nu_\tau$ or $\tau^- \rightarrow K^- K^+ K^- \nu_\tau$ where events with K_S^0 have been excluded. After events are selected the invariant mass distributions are analyzed. The $\tau^- \rightarrow h^- h^+ h^- \nu_\tau$ backgrounds between the channels caused

by particle mis-identification, referred to as cross-feed throughout this paper, are normalized to the measured branching fractions in BaBar. The cross-feed backgrounds are estimated to be $(0.85 \pm 0.01)\%$ for the $\pi^- \pi^+ \pi^-$ channel, $(38.5 \pm 0.2)\%$ for the $K^- \pi^+ \pi^-$ channel, $(2.9 \pm 0.1)\%$ for the $K^- K^+ \pi^-$ channel and $(27.7 \pm 3.0)\%$ for the $K^- K^+ K^-$ channel, where the uncertainties are from MC statistics. The background fractions from events with an extra π^0 in the candidate samples are estimated to be $(3.6 \pm 0.3)\%$ from $\tau^- \rightarrow \pi^- \pi^+ \pi^- \pi^0 \nu_\tau$ in $\tau^- \rightarrow \pi^- \pi^+ \pi^- \nu_\tau$, $(2.3 \pm 0.4)\%$ from $\tau^- \rightarrow K^- \pi^+ \pi^- \pi^0 \nu_\tau$ in $\tau^- \rightarrow K^- \pi^+ \pi^- \nu_\tau$, $(0.4 \pm 0.1)\%$ from $\tau^- \rightarrow K^- K^+ \pi^- \pi^0 \nu_\tau$ in $\tau^- \rightarrow K^- K^+ \pi^- \nu_\tau$ and less than 5.0% from $\tau^- \rightarrow K^- K^+ K^- \pi^0 \nu_\tau$ in $\tau^- \rightarrow K^- K^+ K^- \nu_\tau$. The non- τ backgrounds amount to less than 0.5% of the events for each channel. An arithmetic subtraction is used to remove the backgrounds from the invariant mass distributions for each channel. Detector effects are then removed using Bayesian Unfolding [7], which has been trained using the signal MC for each decay mode. An efficiency correction, initially obtained from MC and corrected using data control samples, is used to correct for efficiency losses from the event selection for each bin in the invariant mass distribution. When the statistical uncertainty on the MC is below 10% the efficiency is determined using the neighbouring bins. The invariant mass distributions are then normalized to unity. The two-dimensional Dalitz distributions for slices of the three-body invariant mass are background subtracted and then efficiency-corrected. The bin width for the Dalitz plots is chosen to be 25 MeV which is approximately 5 times the resolution of the two-body invariant masses. The systematic uncertainties in this work that are taken into account include: the MC signal and background statistics, the potential biases resulting from the Bayesian Unfolding, the uncertainties related to particle identification, the uncertainties in the modeling of the EMC and tracking response, the modeling of the trigger, the luminosity and the modeling of the backgrounds.

For the $\tau^- \rightarrow \pi^- \pi^+ \pi^- \nu_\tau$ it can be seen that invariant mass $M(\pi^- \pi^+ \pi^-)$ is consistent with previous measurements [19]. The width of the $a_1(1260)$ observed in this study is larger than in Tauola [20]. It can also be seen that the $a_1(1260)$, which primarily decays through $\pi\rho$, is distorted by phase space constraints and in particular it can be seen that there is a large discrepancy between the data and the models in the low $M(\pi^+ \pi^-)$ region. The uncertainties of the unfolded $\tau^- \rightarrow \pi^- \pi^+ \pi^- \nu_\tau$ spectra are limited by the particle-id and the relative background fraction.

The $M(K^- \pi^+ \pi^-)$ invariant mass distribution for $\tau^- \rightarrow K^- \pi^+ \pi^- \nu_\tau$ has been measured previously by the OPAL, ALEPH, Belle [19] and CLEO collaborations, where all but the latter unfolded the invariant mass spectrum. The LEP experiments and CLEO had limited statistics and are consistent both with the Belle results and the results presented here. However, the Belle results [19] for the invariant mass distribution and the results presented here are inconsistent. The discrepancy is most pronounced in the 1.4-1.7 GeV/c² range where the $\tau^- \rightarrow \pi^- \pi^+ \pi^- \nu_\tau$ background dominates, indicating that the difference is probably related to the estimate of this background. This hypothesis is consistent with the observed discrepancies in the $\tau^- \rightarrow \pi^- \pi^+ \pi^- \nu_\tau$ branching fraction. The channel $\tau^- \rightarrow \pi^- \pi^+ \pi^- \nu_\tau$ is observed to decay primarily through

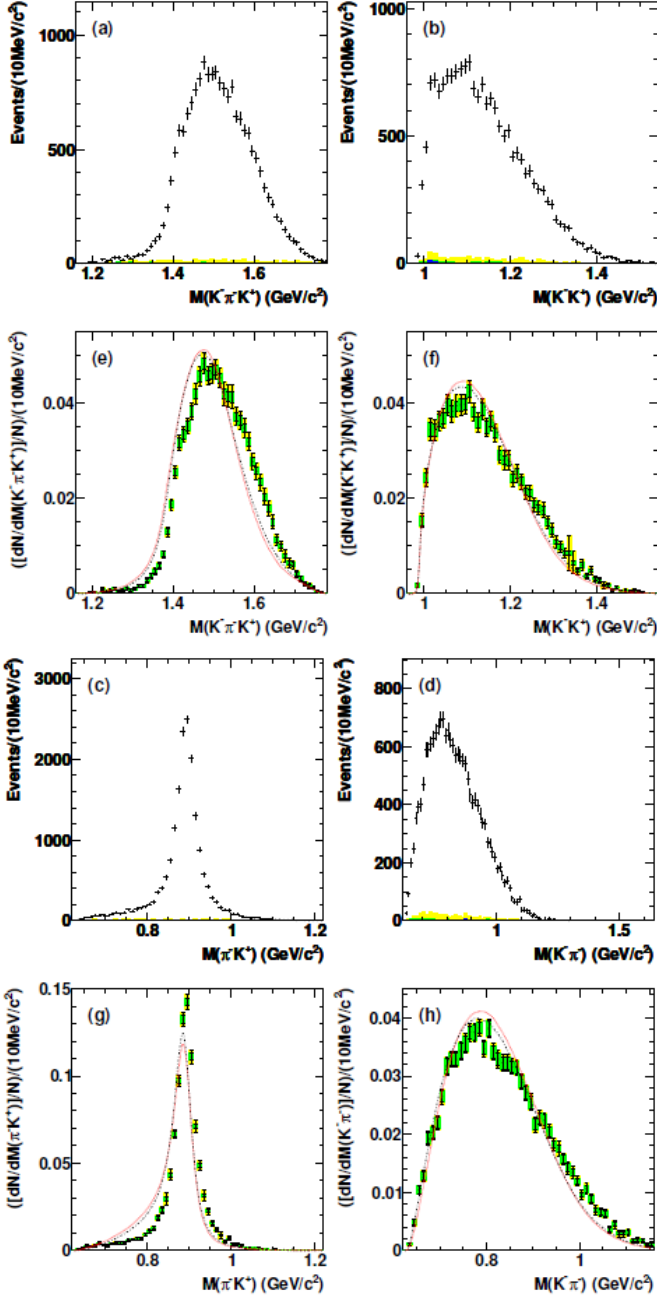


Figure 6: The reconstructed and unfolded invariant mass spectra for the $\tau^- \rightarrow K^- \pi^+ \pi^- \nu_\tau$ channel. We present the reconstructed invariant mass distributions for (a) $M(K^- \pi^+ K^+)$, (b) $M(K^- K^+)$, (c) $M(\pi^- K^+)$ and (d) $M(K^- \pi^-)$ and the unfolded invariant mass spectra (e) $M(K^- \pi^- K^+)$, (f) $M(K^- K^+)$, (g) $M(\pi^- K^+)$ and (h) $M(K^- \pi^-)$. For the reconstructed mass plots, the data is represented by the points with the error bars representing the statistical uncertainty. The blue (dark) histogram represents the non- τ background MC, the green (medium dark) histogram represents the τ backgrounds excluding the $\tau^- \rightarrow K^- \pi^+ \pi^- \nu_\tau$ cross-feed which are represented by the yellow (light) histogram. For the unfolded mass plots, the data is represented by the points with the inner error bars (green) representing the statistical uncertainty and the outer error bars (yellow) representing the statistical and systematic uncertainties. The integral of the unfolded distribution is normalized to unity. The black dashed line is the generator level MC distribution used in the BaBar simulation. The red dotted line is the CLEO tune for Tauola 2.8 [20].

the $K_1(1270)$ and $K_1(1400)$ resonances, and then subsequently through the intermediate states $K^*(892)\pi^-$ and $\rho^0 K^-$. This

general decay structure is consistent with the measurements in [21]. It can also be observed that the ρ^0 which primarily comes from the $K_1(1270)$ is strongly constrained by phase space.

The $M(K^- K^+ \pi^-)$ invariant mass distribution for $\tau^- \rightarrow K^- K^+ \pi^- \nu_\tau$ is consistent with the distribution in [19] for most of the invariant mass spectrum except for a slight excess in the region, 1.65-1.75 GeV/c^2 . This is where the Belle measurement has a large relative cross-feed contribution [19]. The primary decay mechanism is observed to be through $K^*(892)K^-$. In contrast to the $\tau^- \rightarrow \pi^- \pi^+ \pi^- \nu_\tau$ and $\tau^- \rightarrow K^- \pi^+ \pi^- \nu_\tau$ channels, the $\tau^- \rightarrow K^- K^+ \pi^- \nu_\tau$ spectra are statistically limited and therefore do not have as strong of correlation as the aforementioned spectra have. However, there is still a dependence of the $K^*(892)$ resonance on the phase space due to the normalization.

The $\tau^- \rightarrow K^- K^+ K^- \nu_\tau$ decay has been measured by Belle [19] and by BaBar [22]. The $M(K^- K^+)$ invariant mass was shown to decay predominantly through the ϕ resonance and with an upper limit of $B(\tau^- \rightarrow K^- K^+ K^- \nu_\tau) < 2.5 \times 10^{-6}$ at 90% CL [22]. The shape of the $M(K^- K^- K^+)$ distribution is consistent with the only other measurement [19], however, the branching fractions measured by BaBar [22] and Belle [19] are inconsistent by more than 5.4σ .

References

- [1] S. Banerjee, B. Pietrzyk, J.M. Roney, Z. Was, *Phys. Rev. D* **77**, 054012 (2008).
- [2] J. P. Lees *et al.* (BABAR Collaboration), *Phys. Rev. D* **85**, 031102 (2012).
- [3] J. Beringer *et al.* (Particle Data Group), *Phys. Rev. D* **86**, 010001 (2012).
- [4] J.P. Lees *et al.* (BABAR Collaboration), *Phys. Rev. D* **86**, 092010, (2013).
- [5] N. Cabibbo, *Phys. Rev. Lett.*, **10**, 531533, (1963).
- [6] E. Gamiz, M. Jamin, A. Pich, J. Prades, F. Schwab, *Phys. Rev. Lett.*, **94**, 011803, (2005).
- [7] G. D'Agostini, *Nucl. Instrum. Meth.*, **A362**, 487498, (1995).
- [8] B. Aubert *et al.* (BABAR Collaboration), *Nucl. Instr. Methods Phys. Res., Sect. A* **479**, 1 (2002).
- [9] B. Aubert *et al.* (BABAR Collaboration), *Phys. Rev. Lett.* **99**, 021603 (2007).
- [10] B. F.Ward, S. Jadach, Z.Was, *Comput. Phys. Commun.* **130**, 260 (2000).
- [11] S. Jadach, Z. Was, R. Decker J. H. Kuhn, *Comput. Phys. Commun.* **76**, 361 (1993).
- [12] T. Sjostrand, *Comput. Phys. Commun.* **82**, 74 (1994).
- [13] E. Barberio and Z. Was, *Comput. Phys. Commun.* **79**, 291 (1994).
- [14] S. Agostinelli *et al.* (GEANT4 Collaboration), *Nucl. Instr. Methods Phys. Res., Sect. A* **599**, 250 (2003).
- [15] A. Anastassov *et al.* (CLEO Collaboration), *Phys. Rev. Lett.* **86**, 4467 (2001).
- [16] M. Acciarri *et al.* (L3 Collaboration), *Phys. Lett.* **B 501**, 1 (2001).
- [17] J. Beringer *et al.* (Particle Data Group), *Phys. Rev. D* **86**, 010001 (2012).
- [18] S. Nussinov, A. Soffer, *Phys. Rev. D* **80**, 033010 (2009).
- [19] M. Lee *et al.*, *Phys. Rev.*, **D81**, 113007, (2010).
- [20] P. Golonka, B. Kersevan, T. Pierzchala, E. Richter-Was, Z. Was, *et al.*, *Comput. Phys. Commun.*, **174**, 818835, (2006).
- [21] G. Abbiendi *et al.*, *Eur.Phys.J.*, **C13**, 197212, (2000).
- [22] B. Aubert *et al.*, *Phys. Rev. Lett.*, **100**, 011801, (2008).

